J Mater Sci (2009) 44:4342–4347
DOI 10.1007/s10853-009-3648-8

Study of dilute Al–Cu solidification by cooling curve analysis

Osvaldo Fornaro · Hugo A. Palacio

Received: 23 February 2009 / Accepted: 27 May 2009 / Published online: 1 July 2009

Abstract The solidification path of a dilute Al–Cu alloy was studied using controlled solidification conditions and thermal analysis. Under equilibrium considerations, below the limit of maximum solubility, a unique α phase is expected, rounded by rich non eutectic composition. However, the precipitation of the second phase θ is present even for dilute compositions, fundamentally favored by segregation in the liquid and instabilities in the front of solidification. This effect has technological and academic implications, related to the precipitation of intermetallic compounds from the melt.

Introduction

The academic and technological importance of Al–Cu alloys is well known. Moreover, dilute Al–Cu alloys have a hardening effect related to the solution and posterior precipitation of a coherent θ phase [1, 2] in alloys with composition bellow the maximum solubility limit. In the case of cast alloys, it is not possible to avoid the presence of θ precipitates of great size during pouring of bulk pieces. In this case, the solution of these precipitates take very long time as a direct consequence of the structure and the cooling rate of solidification [3–6].

Solidification of hypoeutectic Al–Cu alloys tends to form a characteristic dendritic microstructure of α primary phase, and in this way enclosing eutectic composition. For compositions below the maximun solubilty limit, this eutectic could be considered as non-equilibrium eutectic, and its fraction depends on local solidification conditions [7]. In directional solidification experiences of Al–0.2 and 0.5 wt%Cu [8] it was demonstrated that the presence of the θ phase conforming the eutectic of Al + Al_2Cu composition was responsible for inhomogeneities in the interdendritic liquid, in such a way that cellular walls result in different composition profiles. This results in a characteristic irregular cell morphology in dilute Al–Cu alloys.

Thermal analysis is a classical method for studying metals and alloys solidification [9–11]. By melting and freezing an alloy and registering the temperature–time curves, several characteristical behaviors can be determined [9, 12, 13]. As a cooling curve reflects a balance between the evolution of heat in the sample and the heat flow away from the sample, the start of solidification is easily determined by the latent heat associated to the liquid–solid transformation. Some other variations on the curve can be related to other processes, reactions, and of course the end of solidification [9]. Although differential thermal analysis (DTA) [14] is often used in solidification studies, in the last years computer-aided cooling curve analysis (CA-CCA) has been used for determination of thermo-physical properties and solidification path of metallic alloy [15, 16]. This approach has proved useful in

O. Fornaro
Consejo Nacional de Investigaciones Científicas y Técnicas (CONICET), Av. Rivadavia 1917, Buenos Aires C1033AAJ, Argentina

H. A. Palacio
Comisión de Investigaciones Científicas de la Provincia de Buenos Aires (CICPBA), 526 e/10 y 11, La Plata B1096APP, Argentina

O. Fornaro (✉) · H. A. Palacio
Instituto de Física de Materiales Tandil (IFIMAT), Facultad de Ciencias Exactas, Universidad Nacional del Centro de la Provincia de Buenos Aires, Pinto 399, Tandil B7000GHG, Argentina
e-mail: ofornaro@exa.unicen.edu.ar

other aluminum alloy systems such as grain refinement hipoeutectic Al–Si alloys and commercial Al alloys casting [6, 16].

In analytical form

$$\frac{dQ}{dt} = m\left[fC_P^S + (1-f)C_P^L\right]\frac{dT}{dt} + m\Delta H_f\frac{df}{dt} \quad (1)$$

where m is the mass of the sample, $C_P^{S,L}$ are the heat capacity in solid and liquid, respectively, $\frac{dT}{dt}$ is the cooling rate of the process, ΔH_f is the latent heat of solidification, and f is the fraction of formed solid. Also, Eq. 1 can be written as

$$\frac{dQ}{dt} = m\left[fC_P^S + (1-f)C_P^L + \Delta H_f\frac{df}{dT}\right]\frac{dT}{dt} \quad (2)$$

where $\frac{dQ}{dt}$ is constant and represents the external heat flow imposed externally to the system. It can be seen in these equations that as the parenthesis increases its value during the solidification due to the fact that $\frac{df}{dt}$ is positive, $\frac{dT}{dt}$ must change to sustain the energy balance [9].

In Eqs. 1 and 2, $\frac{dQ}{dt}$ can be evaluated while $f \equiv 0$, i.e., while liquid is cooling if m and C_P^L is known. Also C_P^S can be used for the solid phase by making $f = 1$ and $\frac{df}{dt} = 0$, but the calculus could involve solid state reactions, too.

Then, $\frac{df}{dt}$ or $\frac{df}{dt}$ can be evaluated from (1) and (2). Note that in the general case where $C_P^S \neq C_P^L$, a differential first order equation must be resolved [13] to find $\frac{df}{dt}$,

$$\frac{df}{dt} = \frac{1}{m\Delta H_f}\left[\frac{dQ}{dt} - m\left(fC_P^S + (1-f)C_P^L\right)\frac{dT}{dt}\right] \quad (3)$$

However, it is usual to consider that $C_P^S = C_P^L$ for calculation purposes (see Table 1), in which case the previous equations can be simplified as

$$\frac{df}{dt} = \frac{1}{m\Delta H}\left[\frac{dQ}{dt} - mC_P\frac{dT}{dt}\right] \quad (4)$$

which can be easily evaluated graphically. Although this approximation is not strictly true, it does not involve an important loss of precision in the zone where solidification takes place.

In the cases where more than one reaction is expected, all previous equations must be modified to include the observed behavior, but note that these different contributions would be in the form of the last term of Eq. 2 to reflect changes in the $\frac{dT}{dt}$ curve.

On the other hand, it is known that the actual *liquidus* temperature, as well as the *solidus* temperature, depend on cooling rate due to kinetic effects during crystal growth. To find correct liquidus temperature at equilibrium conditions, the obtained values are often plotted against the square root of cooling rate and the fitted values extrapolated to zero cooling rate. *Solidus* temperature changes in a more important rate than *liquidus* temperature, due to microsegregation effects during solidification. In alloys where the eutectic is formed through an intermetallic second phase, like Al–Cu or Al–Si, the microsegregation increases the liquid inhomogeneities allowing for the formation of these phases in the interdendritic spacing, even for dilute compositions. This can be noted because the clustering of a θ phase decreases the effective composition of free interdendritic liquid. This effect was discussed in a previous work, under directional solidification experiments [8], and it also has a great significance during the precipitation of secondary phases during the casting of technological alloys and in thermal treatments design.

The aim of this work is to study the solidification path of dilute Al–Cu alloys by showing the presence of a precipitation of a second phase even for low composition alloys, in such a way that a change in the expected solidification path takes place.

Table 1 Heat Capacity of Aluminum as a function of temperature [17]

T [K]	373	473	573	673	933–1173
$C_P^{S,L}$ [J/Kg K]	938	984	1030	1076	1080

Experimental setup

The alloys used were melted from purity elements in a SiC crucible under Ar atmosphere. The cylindrical preingots were poured into a graphite mold. These cylinders were then used in the cooling curves, by melt and solidification at different cooling rates at the time the temperature–time recordings were taken.

The solidification setup consists of a 1.5 KW electric furnace, with an electronic temperature controller that permits linear ascending or descending temperature ramps from 0.1 to 10 K/min. The samples of approximately 5 to 10 g were located in the furnace, melted, and solidified at controlled cooling rates. The temperatures of furnace and samples were taken with calibrated K thermocouples and

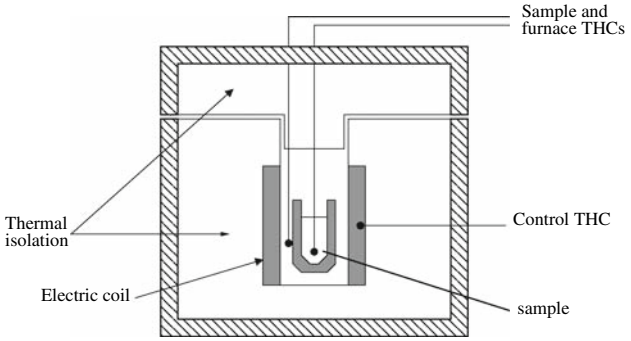

Fig. 1 Schematic setup used for the cooling curves determination

measured simultaneously with a NI-USB 9211A interface connected to a personal computer. The schematic setup used to obtain cooling curves can be seen in Fig. 1.

After solidification, the samples were metalographically observed by optical microscopy. For such a purpose, they were cut and mechanically and electrolytically polished by using traditional methods, and revealed by chemical etching [8].

Results and discussion

The upper part of Fig. 2 shows a typical cooling curve obtained for Al–4 wt%Cu at a cooling rate of 10 K/min = 0.16 Ks^{-1}. Over this curve it is possible to observe that as the temperature decreases, a first change appears due to the initial formation of α phase. Note that the derivative curve shown at the lower part of the same figure, shows a clear variation at this point, indicating the start of the nucleation. This curve was obtained numerically from $T-t$ data collected during the experience. As freezing progresses, the temperature stabilizes at the liquidus temperature $T_{liquidus}$. After that, a cooling zone starts, reaching the external heat extraction curve, and finally, an isothermal, eutectic reaction is noted.

It is important to note that, for compositions below the maximum solubility limit, a homogeneous α phase is expected, at least for small enough cooling rates. However, the microsegregation present in front of the formed solid causes liquid inhomogeneities, in such a way that, in some sites, it could promote an initial formation of the second phase, θ in this case. This formation could be evident in the change of derivative curve behavior, after the initial α-formation stage, where a second transformation arises.

In Fig. 3, $\frac{dT}{dt}$ is represented as a function of the temperature for solidification at different cooling rates. The derivative $\frac{dT}{dt}$ is used to evaluate Eqs. 1–3. This representation is useful to compare the solidification behavior at different cooling rates. Please remember that solidification proceeds from right to left in these figures, as temperature decreases during the solidification process. In this figure it can be seen that the fundamental aspect of the curves look similar at different cooling rates, and the main differences are related to the change in the values of $T_{liquidus}$ and $T_{solidus}$. The first appears as almost constant temperature or *plateau* in the temperature–time plot, meaning that it looks constant in the derivative. It is possible to observe an important change in the derivative at the beginning of nucleation, occurring at approximately the same temperature for all the cooling rates under study, reaching different values of liquidus temperature. This behavior suggests that nucleation starts with different rates but at the same temperature. As solidification proceeds, the derivative reaches a local minimum at solidus temperature. Finally, there is evidence of the isothermal eutectic reaction of the remaining liquid. The range of solidification is between the beginning of nucleation and this eutectic transformation.

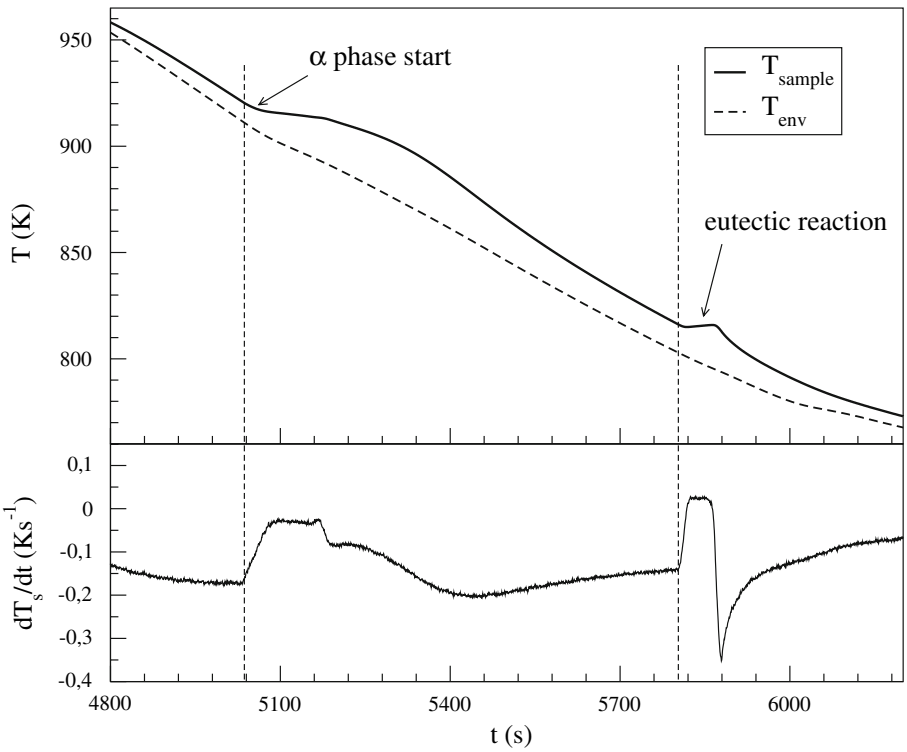

Fig. 2 Cooling curve of Al–4%Cu, 0.16 Ks^{-1}

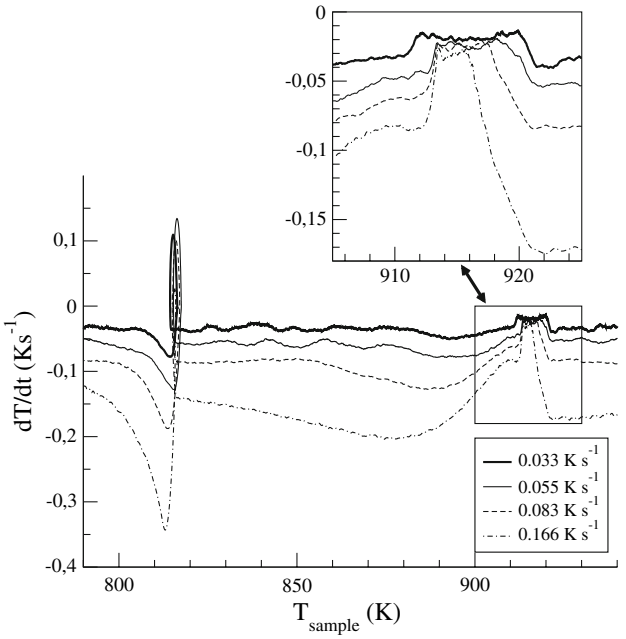

Fig. 3 $\frac{dT}{dt}$ in function of sample temperature and cooling rate, Al–4%Cu

The excerpt of Fig. 3 shows the zone where the solidification of the samples starts with a higher level of detail. In this figure it is clear that the jump in the derivative begins at a similar temperature, independently of the cooling rate. This jump is an effect of latent heat liberation during nucleation events, but the nucleation rate depends on the solid fraction, which varies with cooling rate. The result is different slopes of the $\frac{dT}{dt}$ in the plot, as can be seen in the figure. When the solidification of α phase is completed, a decreasing in $\frac{dT}{dt}$ is expected, because the term responsible for nucleation in Eq. 2 disappears. However, as can be seen in Figs. 2 and 3, another thermal event appears below the main transformation. This effect was more evident at high cooling rates because the maximum is shifted to higher temperatures as cooling rates decrease, overlapping with the contribution of the α nucleation. This effect could be promoted by nucleation in the liquid ahead of the interface due to supercooling. These nuclei could be responsible in many cases for equiaxed grain formation. When solidification proceeds under small cooling rates conditions, only the formation of the α phase is detected. In all cases, these processes enclose rich liquid in the interdendritic spacing, that finally solidify with an eutectic reaction, in such a way that it is not possible to avoid the formation of the second phase. Figure 4a shows the microstructure of a sample solidified at a rate of 0.16 Ks^{-1}. It is possible to observe the typical structure of α phase dendrites trapping interdendritic $\alpha + \theta$ eutectic. At lower cooling rates the structure does not change fundamentally,

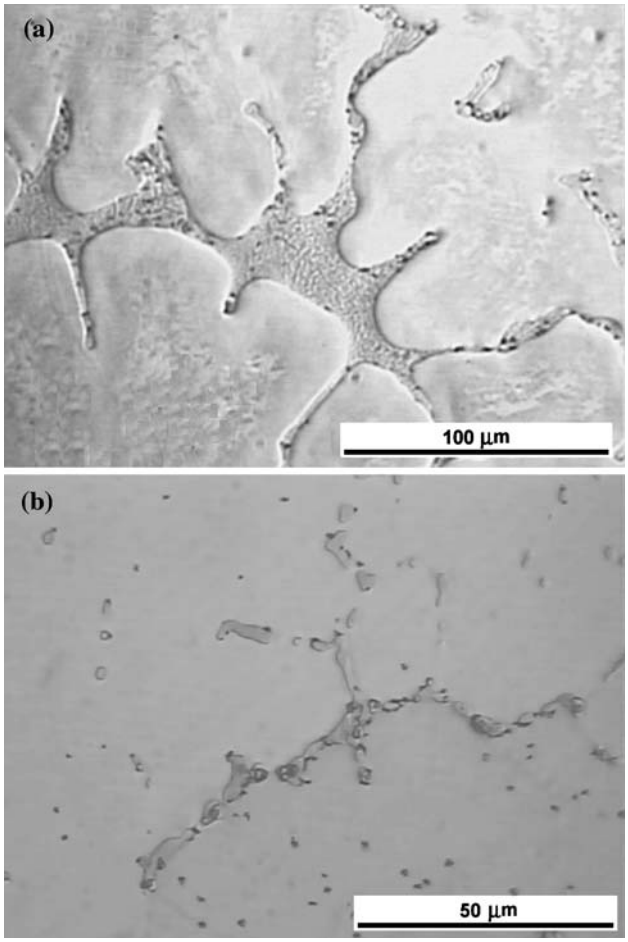

Fig. 4 Typical micrograph of α dendrites and $\alpha + \theta$ interdendritic eutectic, for Al–4%Cu cooled at **a** 0.16 Ks^{-1} ; **b** 0.033 Ks^{-1}

but it can be noted that the quantity of trapped eutectic is lesser, as Fig. 4b shows.

A subsequent analysis using a minor composition of Al–2.5%Cu, allowed us to find a general similar qualitative behavior. A first arrest appears clearly in *T–t* curve and is due to the solidification of the α phase, as Fig. 5 shows. As solidification continues, the eutectic transformation of remaining intercellular liquid is almost imperceptible in this curve. The lower part of the same figure shows the derivative $\frac{dT}{dt}$ as a function of time. This representation shows well-defined changes both at the start of solidification, and also at the end, where a minimum can be observed. This is not the actual equilibrium *solidus* temperature, because a small remaining rich liquid is trapped between α cells or dendrites. By representing the derivative as a function of temperature, as shown in Fig. 6, these effects are more evident. When solidification starts, the liberation of latent heat appears at one temperature, showing that the plateau in *T–t* curve is more plane due to a lesser composition, the solidification of α is almost isothermic in the first stage. The eutectic reaction can also be

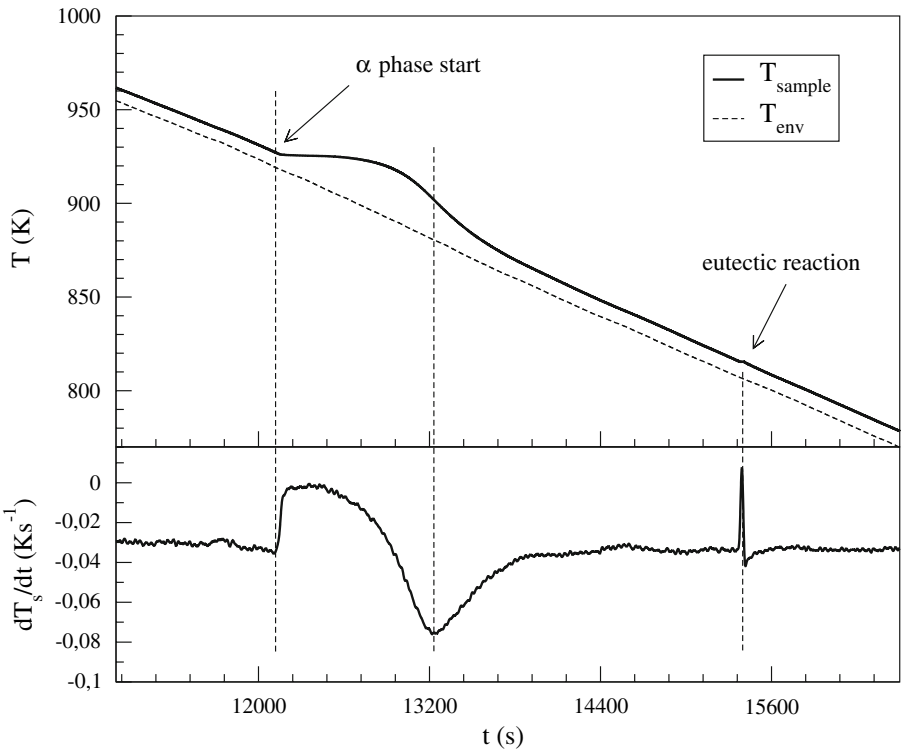

Fig. 5 Cooling curve of Al–2.5%Cu at 0.033 Ks^{-1}

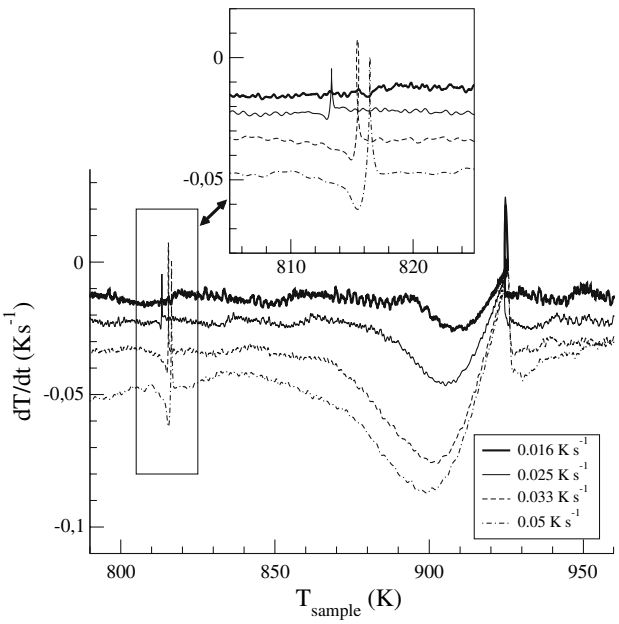

Fig. 6 $\frac{dT}{dt}$ in function of sample temperature and cooling rate, Al–2.5%Cu

seen, shown as a second peak. By decreasing the cooling rate the eutectic reaction is less evident, as finally disappeared at the cooling rate of 0.016 Ks^{-1}. After this last reaction, the baseline of the derivative reaches the cooling rate externally imposed. Figure 7 shows the microstructure of the samples solidified at different cooling rates. In the first micrograph at 0.05 Ks^{-1} the cellular microstructure appears well defined, as cellular walls are clearly visible. In some of the walls, a quantity of interdendritic liquid had finally solidified forming eutectic composition. In the second at 0.016 Ks^{-1}, cellular walls are less evident, but it is still possible to see some evidence of eutectic composition in the structure forming nodes.

As an application example, the solid fraction for the Al–2.5%Cu alloy is calculated and represented in Fig. 8, which shows that the solid fraction grows quickly after solidification begins, reaching an asymptotic value close to 1 at the eutectic temperature. In the cases where the solidification ends with a final eutectic reaction, a small vertical shift appears at such temperature. In our case, the smaller cooling rate of 0.016 Ks^{-1} does not show evidence of eutectic reaction. In the same figure, a standard Scheil calculus for f_s is included, showing a similar behaviour to the higher cooling rates.

Conclusions

Controlled solidification experiences were carried out to study the path of solidification of Al–Cu alloys with composition below maximum solubility limit. The thermograms achieved show that for the greater composition alloy under study, another nucleation event appears simultaneously with the first solidification stage. This effect is more evident at a greater cooling rate of solidification and could evidence equiaxed grain formation in the liquid ahead the interface.

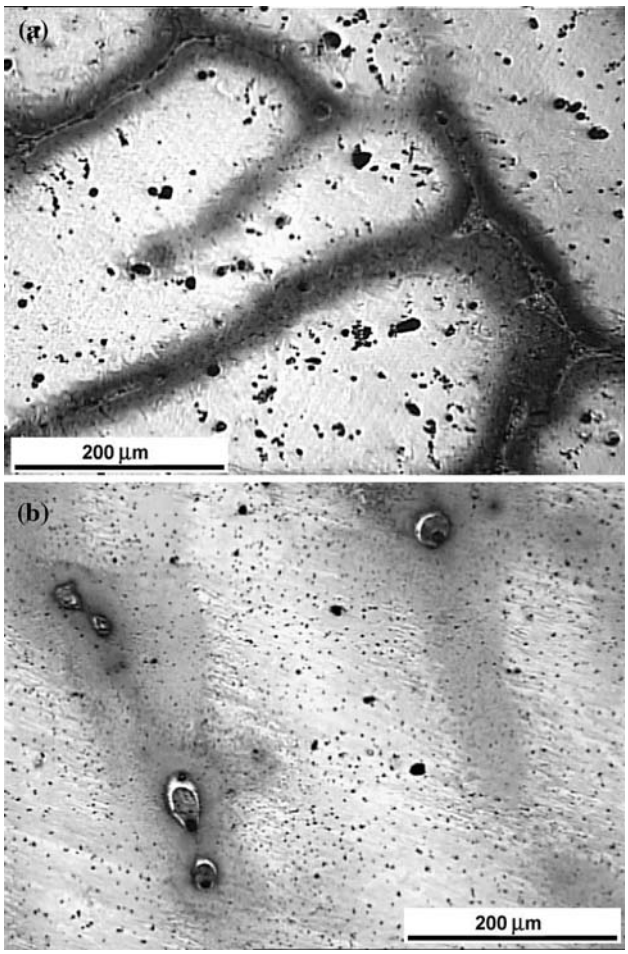

Fig. 7 Al–2.5%Cu micrographs at different cooling rate. **a** 0.05 Ks^{-1}; **b** 0.016 Ks^{-1}.

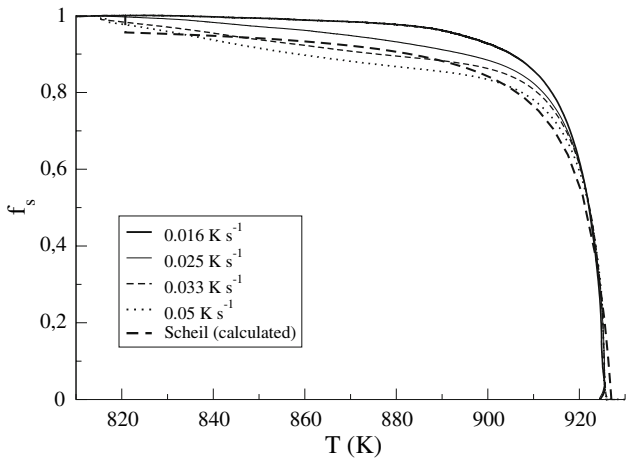

Fig. 8 Solid fraction calculated from experiments for Al–2.5%Cu at different cooling rates

In general, solidification starts with cellular or dendritic microstructure of the α phase, enclosing rich interdendritic liquid, and then finally forming a second θ phase and then $\alpha + \theta$ eutectic. However, in the samples of small cooling rate, there is no evidence of eutectic reaction in the cooling curves, although it appears in small quantities in the microstructure. In this case, the heat associated with this reaction maybe small compared to the measuring noise.

Acknowledgements This work was carried out at IFIMAT (CIC-PBA-MT, UNCPBA) and supported by SeCAT-UNCPBA, ANPCyT, CONICET, and CICPBA. We also appreciate the technical support given by O. Toscano at Thecnical Department of IFIMAT during the design of the equipment.

References

1. Mondolfo LF (1979) Aluminum alloys: structure and properties, 1st re-edn. Butterworth, London, Boston
2. Papazian JM (1981) Metall Trans A 12:259
3. Singh SN, Bardes BP, Flemings MC (1970) Metall Trans A 1:1383
4. Fuchs EG, Roósz A (1972) Metall Trans A 3:1019
5. Ouellet P, Samuel FH (1999) J Mater Sci 34:4671. doi: 10.1023/A:1004645928886
6. Faraji M, Todd I, Jones H (2005) J Mater Sci 40:6363. doi: 10.1007/s10853-005-3103-4
7. Kasperovich G, Volkmann T, Ratke L, Herlach D (2008) Metall Mater Trans 39A:1183
8. Fornaro O, Palacio HA, Biloni H (2006) Mater Sci Eng A 417:134. doi:10.1016/jmsea.2005.11.013
9. Fredriksson H (1988) In: Metals handbook, Casting, 9th edn, vol 15. ASM Int., Materials Park, OH, USA, p 182
10. Biloni H, Boettinger WJ (1996) In: Cahn RW, Haasen P (eds) Physical metallurgy, 4th edn, vol II. Elsevier Science Publishers, Amsterdam, p 669
11. Barlow JO, Stefanesku DM (1997) AFS Trans 105:349
12. Shabestary SG, Ghodrat S (2007) Mater Sci Eng A 467:150
13. Gibbs JW, Mendez PF (2008) Scr Mater 58:699
14. Boettinger WJ, Kattner U (2002) Metall Mater Trans 33A:1779
15. Wang Q, Li YX, Li XC (2003) Metall Mater Trans 34A:1176
16. ul haq I, Shin J-S, Lee, Z-H (2004) Met Mater Int 10:89
17. Smithells CJ, Brandes EA (eds) (1976) Metals reference book, 5th edn. Butterworth, London, Boston